Ocean Engineering 96 (2015) 215–225

Contents lists available at ScienceDirect

Ocean Engineering

journal homepage: www.elsevier.com/locate/oceaneng

Effect of shroud on the performance of horizontal axis hydrokinetic turbines

Mohammad Shahsavarifard, Eric Louis Bibeau *, Vijay Chatoorgoon

Department of Mechanical Engineering, University of Manitoba, Winnipeg, MB, Canada R3T 5V6

ARTICLE INFO

Article history:
Received 14 May 2014
Accepted 8 December 2014

Keywords:
Hydrokinetic turbines
Shrouds
Horizontal turbines
Turbine efficiency

ABSTRACT

The idea of wind turbine power enhancement by means of a shroud has been investigated for decades with no commercial success. However, due to some beneficial aspects, shrouds are poised to serve the hydrokinetic turbine industry. We report on the experimental measurements performed in a water tunnel on a 19.8 cm diameter horizontal axis hydrokinetic model turbine utilizing two shrouds. Power and thrust coefficients of the model turbine with and without the shrouds investigated are obtained over the range of the power curve. A maximum power enhancement of 91% over the unshrouded turbine is obtained with one of the shrouds. Maximum power coefficients are recalculated based on the maximum area of shroud and are found to be comparable to that of the unshrouded turbine. At flow speed of 1 m/s, an extended blade that generates the same power as the shrouded turbine is found to have a diameter equal to the diameter of the shroud exit. This aspect is critical as the use of shrouds contrary to much of the literature is not to increase the hydrokinetic turbine efficiency, but to gain advantages in the powertrain design, and have the turbine power less impacted by changes in the flow direction.

1. Introduction

The growing worldwide energy demand, finite resources of fossil fuels and regulations to control greenhouse gases are just a few reasons to motivate energy markets to extend the use of renewable energies. Hydrokinetic energy of water streams is a source of renewable energy and countries like Canada could generate part of their electricity from it. Horizontal axis hydrokinetic turbines are amongst the devices used to extract hydrokinetic energy (Khan et al., 2009). Horizontal axis hydrokinetic turbines work on the same principals as wind turbines. A lift force generated as a result of fluid flowing on the rotor blades produces torque on the turbine shaft which is then converted into electricity by a generator. Originating from gravitational forces, behaviour of water currents is more predictable than wind caused by atmospheric changes. This leads to a reliable and predictable power generation from water currents. In contrast to the conventional hydroelectric power generation that needs dam to provide water head, in this method turbines are placed in rivers or ocean streams and generate electricity without making significant change to the environment (O Rourke et al., 2010).

The relatively low power density of hydrokinetic energy however is a drawback. Diffuser augmented wind turbines have been investigated for more than fifty years as a remedy in wind industry (van Bussel, 2007). Phillips (2003) reviewed the theoretical, experimental, and numerical studies done to the date for making the idea commercially viable. However, a successful commercial unit hasn't been introduced in the market due to high loads exerted on the duct, heavy support structure needed, and expensive yawing mechanism. This added complexity along with its prohibitive cost compared to the simple method of extending the rotor diameter is the main reason preventing commercial use of the idea (Shives and Crawford, 2011). Continuous technological achievements in mechanical engineering, material science and manufacturing techniques enable construction of larger size blades. This superseded the diffuser augmentation in wind turbine industry, as there is relatively no space limitation for installing larger turbines in the atmosphere. Nevertheless, diffuser augmented wind turbine is still subject of some studies confined to academia: to mention just three, Isensee and Abdul-Razzak (2012), ten Hoopen (2009) and Ohya et al. (2008) have recently done numerical and experimental studies in this field.

Together with the rising efforts to take advantage of kinetic power of water streams the idea of shrouded turbines is becoming prevalent. It is assumed that due to some beneficial aspects water currents have compared to wind, a shroud has the potential to benefit hydrokinetic turbine designs. The velocity and direction of water streams are practically fixed and seasonal changes are more predictable than changes in the wind. This eliminates the need for yawing mechanism and reduces the extreme loads due to storm

* Corresponding author.
E-mail address: bibeauel@cc.umanitoba.ca (E.L. Bibeau).

http://dx.doi.org/10.1016/j.oceaneng.2014.12.006
0029-8018/

Fig. 1. Clean Current's diffuser, oblong in cross section at the exit, combines the benefits of maximizing the blade diameter for peak performance with containment of the rotating blades to prevent accidental impact on marine life (left), and the turbine being deployed in the Winnipeg River to field test in a remote community application using local equipment (right). (Photos courtesy of Clean Current).

conditions on the shroud (Khan et al., 2008). A shroud, in addition to its contribution to power enhancement, can contribute to the support structure to install the turbine on the riverbed for instance, or as casing for components of the turbine generator (Drouen et al., 2007). A few works have been reported in the open literature on shrouded horizontal axis turbines for water current applications.

In the absence of a consistent theory for choosing the inlet and outlet to the turbine (Lawn, 2003), different designs of shroud with different yet inconsistent results on the effectiveness of shroud are reported. Lawn (2003) studied shrouded turbines using a one-dimensional theory that treats ducts as contractions or expansions upstream or downstream of the turbine. He shows that an enhancement of more than 30% in power coefficient can be gained over the optimum for an unshrouded turbine. It is also concluded that significantly greater power enhancement in the literature is associated with non-optimum conditions for the unshrouded turbine. Gaden (2007) studied power enhancement of hydrokinetic turbines with shroud using 3-D CFD simulations. He modeled the rotor using rotating reference frame model and tested different configurations for shroud. A shroud with a cylindrical inlet and 20° half angle diffuser with exit area ratio of 1.56 is found to enhance the power by factor of 1.5. It is further stated that a cylindrical inlet degrades the turbine performance. Gaden and Bibeau (2010) modeled turbine rotor as a momentum source region and found the enhancement factor of 3.1 for the same shroud in the former study. The inconsistency in enhancement factors between the two studies is stated to be due to the different methods used to model the rotor. Scherillo et al. (2011) carried out experimental and numerical studies on shrouded hydrokinetic turbines. Geometry of shroud is obtained in a numerical optimization process to be a diffuser with an airfoil profile having 26° pitch angle and exit to throat area ratio of 1.7. Experiments showed that the maximum power coefficient of the shrouded turbine based on the rotor diameter is enhanced by a factor of 2. This is then stated to be 7.5% increase when power coefficient is calculated based on the diffuser exit area. Shives and Crawford (2011) performed axi-symmetric CFD simulations on a series of shrouds with the turbine rotor modeled as an actuator disk. They studied effect of viscous loss, flow separation and base pressure on the performance behaviour of the shrouds. They conclude viscous loss in the inlet is negligible and flow separation in the diffuser leads to a significant performance loss. They further propose a well-designed duct as a flanged diffuser that creates a large base pressure. Lokocz (2012) carried out experimental studies on shrouded horizontal axis kinetic turbine in a towing tank. The author used two different rotor blade designs for the unshrouded and shrouded turbines and a cylindrical wing of NACA 4412 profile for the shroud model. Experiments showed a slight reduction in the performance of the shrouded turbine. The reason is believed to be the low thrust coefficient of the shroud due to its design. Also, no significant change is seen in the performance of the rotor blade used in shrouded turbine with and without the shroud.

In the area of commercial application diverse designs of shrouded turbines are observed. A number of companies have shrouded kinetic turbines in field test for tidal stream and river applications. Clean Current Power System Inc. develops river and tidal turbines for different water velocities and depths. The largest river turbine with 3.5 m diameter three bladed rotor has a rated power of 65 kW at 3 m/s water speed. The turbine utilizes a 3.1 m long shroud with 3.5 m diameter cylindrical inlet and an oval outlet 3.5 m high and 4.6 m wide. Fig. 1 shows their ducted river turbine being deployed at the Canadian Hydrokinetic Turbine Test Center on the Winnipeg River, using an approach suitable for remote communities. OpenHydro manufactures shrouded open centre tidal turbines with an integrated generator placed in the shroud. They deployed a 1 MW unit in the Bay of Fundy in 2009. Renewable Energy Research fabricates shrouded turbines under the name of TREK. TREK-I with 3.6 m diameter and 7.5 m long shroud weighs 36 t and has a rated power of 340 kW. It needs a minimum of 5.5 m water depth for installation and has a cut-in speed of 1.5 m/s. In 2010 they deployed a TREK-I unit in the Saint Laurence River. Lunar Energy proposes bi-directional tidal turbines with a symmetrical Venturi duct known as Rotech Tidal Turbine. A 1 MW unit weighing 2500 t has 11.5 m diameter rotor and 19.2 m long shroud. It is designed to sit on the seabed at depths of 40 m or more. They designed and patented a 2.4 MW unit in 2012.

This paper describes design of a model horizontal axis kinetic turbine as well as two shrouds and the experimental measurements performed in a water tunnel. This study aims to experimentally quantify the effect of a shroud on the power of hydrokinetic turbines over the entire performance curve with reliable and consistent results. Tests are done at three water speeds and for three turbine configurations: turbine blade alone and then with two shrouds. Output power of the turbine and its thrust force are measured experimentally. Results are corrected using a theoretical model that accounts for free surface proximity and blockage effects of the water tunnel. We present consistent power and thrust coefficient curves obtained for the model turbine and discuss effect of Reynolds number on the power coefficients. Discussions continue to find the size of an extended blade that can generate the same power as the shrouded turbine to put efficiency gains into proper perspective. Finally, some advantages and disadvantages of a shrouded turbine versus extending the rotor blades are discussed.

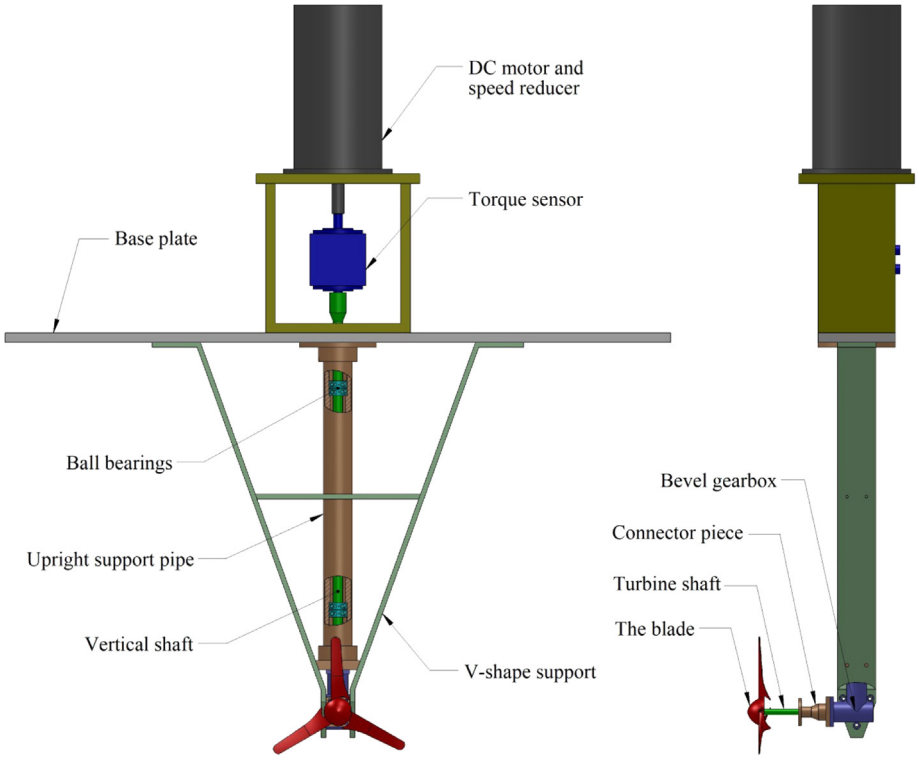

Fig. 2. Front view (left) and side view (right) of the test rig and model turbine without shroud installed. The rotor blade is 19.8 cm in diameter.

2. Experimental setup

2.1. Water tunnel

Tests are performed in the recirculating water tunnel facility at the University of Manitoba. The tunnel has a vertical flow loop configuration with a 61 cm wide by 183 cm long test section. It allows a maximum 60 cm water height in the test section. A single stage, axial flow, propeller pump circulates water in the water tunnel and provides a maximum flow speed of 1.1 m/s at the test section for the full water height. A variable speed motor control adjusts the motor speed and hence the water flow rate. This provides a variable water speed range from zero to the maximum flow speed at the test section. Turbulence intensity of the flow at the test section is less than 3% for the maximum speed.

2.2. Test rig and model turbine

The test rig consists of a base plate that sits on the two sides of the water tunnel upper rim and keeps the model turbine submerged at the center of the flow cross section as well as securing the instrumentation. Locating the rotor hub at the center of the flow cross section gives a clearance of one rotor diameter around the turbine to the tunnel walls and free surface. The model turbine consists of a rotor blade secured to the turbine horizontal shaft. A vertical shaft supported with ball bearings within an upright support pipe connects the horizontal turbine shaft to the instrumentation located above the water tunnel. A right angle 1:1 bevel gearbox couples the turbine shaft to the vertical shaft. The turbine shaft aligns the blade perpendicular to the flow direction one radius upstream of the upright support pipe. This arrangement helps minimize the influence of flow disturbances from the support structure on the turbine performance. Two support flat bars in a V shape secure the turbine and the upright support pipe to the base plate of the test rig. This eliminates turbine vibrations at higher flow and shaft speeds. A connector piece fixed to the bevel gearbox flange enables replacing shrouds around the blade. The turbine shaft and connector piece are designed to position the rotor axially at the least cross sectional area of each shroud: inlet of the diffuser and throat of the shroud. A schematic of the model turbine and the test rig is depicted in Fig. 2.

Table 1
Characteristics of a rotor blade at selected spanwise locations.

r/R	c/R	t/c	Pitch (°)
0.19 (Hub)	0.24	0.14	30
0.60	0.15	0.15	12
0.96	0.12	0.10	4

2.3. The rotor blade

The rotor blade is a 19.8 cm diameter three bladed H0127 wind turbine blade of KidWind Project Inc. The geometric characteristics of the blade inspected visually and measured using a caliper with a 0.02 mm accuracy are as follows. The hub diameter is 19.0% of the rotor diameter and the blade section consists of flat bottom airfoils. The chord, thickness, and pitch angle for selected spanwise locations on the blade are summarized in Table 1. A circular arc of approximately 7.0 mm radius at r/R of 0.96 makes a rounded end at the blade tip. Solidity of the blade is calculated to be 0.13.

2.4. Shrouds

Two shrouds are designed and manufactured to study and compare the effect of shroud on the performance of the model turbine. One is a convergent–divergent duct manufactured in a rapid prototyping machine and is referred to as the *shroud*. The other is a straight wall duct machined out of acrylic block and is referred to as the *diffuser*. Area ratio and half angle for the shroud and the diffuser are selected based on the studies available in the

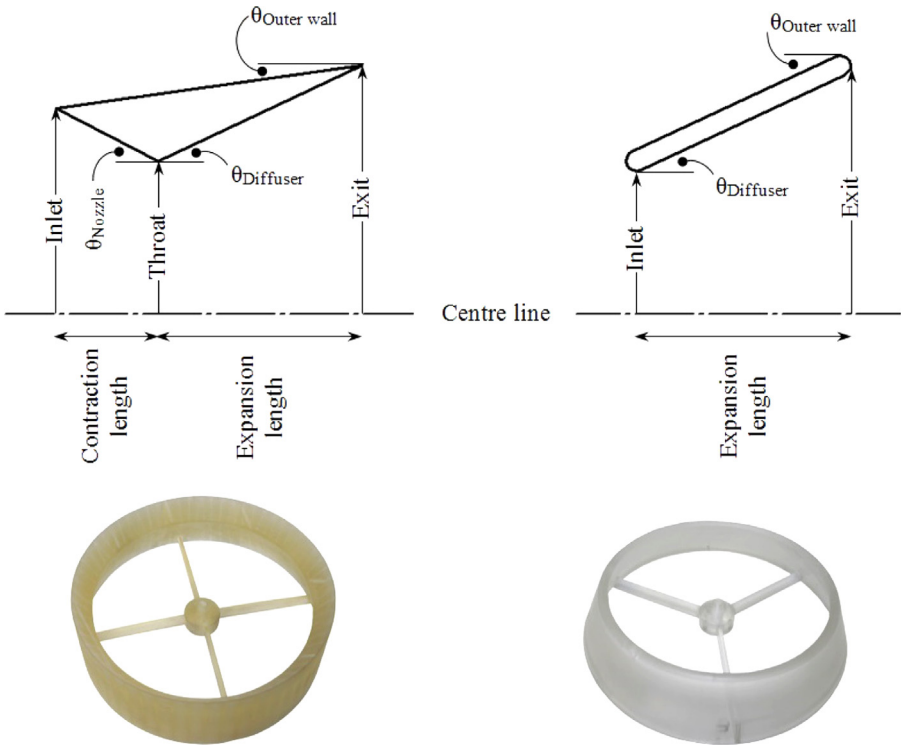

Fig. 3. Schematic profile and picture of the shroud (left) and the diffuser (right).

Table 2
Dimensions of the shroud and the diffuser.

Dimension	Shroud	Diffuser
Inlet diameter (cm)	22.6	20.1
Throat diameter (cm)	20.1	–
Exit diameter (cm)	25.0	25.0
Contraction length (cm)	2.5	–
Expansion length (cm)	5.2	5.2
Nozzle half angle (°)	27	–
Diffuser half angle (°)	25	25
Outer wall angle (°)	8	25

literature. Schematic profiles and pictures of the shroud and the diffuser are depicted in Fig. 3 and the geometric characteristics are summarized in Table 2. The thickness of the diffuser wall is 9.0 mm.

2.5. Selection of area ratios and angles

Two wake regions exist behind a kinetic turbine rotor blade: the near wake and the far wake. The region immediately after the rotor blade called the near wake has influence on the flow field around the rotor and the power extraction of the turbine (Vermeer et al., 2003). The fluid passing the rotor contributes its kinetic energy to the turbine shaft and forms a low energy wake region behind the blade. Fluid in the wake doesn't have sufficient energy to move downstream rapidly and hence blocks the flow passage to the rotor plane. This decreases the fluid mass flow rate to the turbine rotor plane and therefore the extracted power. Another feature of the near wake is tip vortices, generated at the tip of the blades, moving at the expanding boundary of the wake region. Fluid flowing on the blade pressure side tends to roll around the blade tip and go to the low pressure region at the blade suction side. This, known as the tip loss, decreases the pressure difference between the blade surfaces and hence the lift force on the blades, effectively reducing turbine power. The fluid rolls generated around the blade tip then move downstream and form the tip vortices. Ebert and Wood (2002, 1997) conducted experiments to study the near wake of a small wind turbine and conclude that quantities of the flow angular momentum is lost to generate tip vortices. This angular momentum in the absence of tip vortices could be extracted by the turbine rotor and increases the power output. Induced velocities in the rotor plane that affect turbine performance is another phenomenon associated with the tip vortices. Tip vortices are also known to be responsible for rotor noise and blade vibration (Massouh and Dobrev, 2007).

By controlling the destructive behaviour of the near wake and tip vortices, turbine performance improves. This can be done by adding a shroud to facilitate expansion of the slow moving, low static pressure wake behind the rotor. A proper expansion increases static pressure of the flow and provides sufficient kinetic energy to move downstream and clear the passage to the rotor for the entering flow. This arrangement consequently increases flow velocity through the turbine rotor (Hansen et al., 2000). Moreover, a shroud providing a proper size gap between the inner shroud wall and the blade tip prevents tip losses by not letting the upstream flow at the blade to roll around the blade tip. This not only prevents lift force reduction of the blades, but also prevents formation of tip vortices and consequently increases the output power and decreases vibration level and fatigue loads on the rotor. Also, a thin layer of fluid passing through the gap between blade and shroud wall energizes the boundary layer flow at the wall and keeps it attached (Hansen et al., 2000). In our work, a 0.8% of the blade diameter clearance is considered for the gap size.

The area ratio and half angle for the shroud and the diffuser are selected as follows. The exit area ratio is adopted from the CFD optimization work of Gaden (2007). Gaden optimized diffuser half angle and area ratio for higher power and lower drag of turbine. Diffuser area ratio of 1.56 and 20° to 30° half angle are reported as the optimum values and it is concluded that turbine power decreases outside this half angle range. The half angle is stated

to be function of the free stream velocity and is recommended to match the natural flow expansion. To find the expansion path of the flow passing a rotor blade for the present study, several flow visualization works on wind turbine models are reviewed. Alfredsson and Dahlberg (1979) as part of their research studied the wake behind a solid disk and documented a smoke flow visualization study performed in a wind tunnel. The smoke path over the disk shows the expansion of the flow behind it. The expansion angle of the flow measures approximately 25° for a Reynolds number of the order 10^5 based on the disk diameter. van Holten (1981) as part of his work on a general aerodynamic theory for wind energy concentrator systems compares the flow passing a conventional rotor blade and one equipped with tip vanes. Photos of smoke flow visualization show expansion of flow passing both rotors. The angle at which flow expands behind the conventional rotor is 25° as per our measurement. Vermeer (2001) also did smoke flow visualization in a wind tunnel on a 20 cm rotor blade to study wind turbine wakes. The angle at which flow leaves the rotor blade is also 25° from the photos provided in his paper. Tip vortices moving downstream are also clearly visible. Haans et al. (2005) conducted smoke flow visualization to determine tip vortex locations and wake expansion of a model wind turbine rotor at different blade pitch and rotor yaw angles. Experiments are done in Reynolds number of the order 10^5 based on the rotor diameter. Photos of the flow visualization along with the diagrams of tip vortex locations are provided. Results show a range of approximately 18° to 31° for flow expansion angle behind the turbine rotor for different blade pitch angles in axial flow. This is in agreement with the range Gaden and Bibeau (2010) proposed for diffuser half angle based on their numerical optimization study.

Inspecting these studies led the present authors to accept 25° angle as an average value for the natural expansion angle of the flow behind the turbine rotor for hydrokinetic turbines for the Reynolds number range of interest. Therefore, the shroud and the diffuser are designed with 25° divergence angle. An inlet with half length of the diffuser is designed for the shroud to accelerate the flow through the rotor. An inlet also helps improve the uniformity of flow and reduces its unsteadiness across the rotor blade (Lilley and Rainbird, 1956). Based on the results of their study, Lilley and Rainbird (1956) propose that the inlet area ratio, ratio of the inlet to throat area, should not be greater than the exit area ratio–the criterion considered in the design of inlet for the shroud in the present study.

It is worth mentioning that two numerical optimization works have also reported the same diffuser angle. Scherillo et al. (2011) in an axi-symmetric CFD optimization study of a shrouded turbine found 26° as the optimum angle for diffuser. Isensee and Abdul-Razzak (2012) did three dimensional CFD optimization study on diffuser augmented wind turbine and found a diffuser with 25° angle the best to enhance performance of the turbine. Interestingly, different approaches, empirical observation used in this study and numerical optimization by other authors, independently result in the same value for the diffuser angle. It should be noted that these above mentioned works are published after the design and construction of the present shroud and diffuser.

2.6. Instrumentation

Torque and thrust of the turbine rotor is measured for the entire range of the power curve using a torque transducer and a load cell. Generator and variable resistance arrangement are used to extract power of the turbine (Myers and Bahaj, 2006). However, in such a method it is not possible to capture power at low tip speed ratios where blades are in stall state and turbine produces low power. To cover the entire span of the performance curve, the method of a driving motor used by Birjandi et al. (2013) is employed here. In this method, a motor drives the turbine at a constant speed with the torque transducer placed between the motor and the turbine, as shown in Fig. 2. This arrangement enables to measure the torque at any tip speed ratio. In this study, we use a 0.25 HP AC motor coupled to a 1:2 speed reducer. Reducing the motor rpm provides the torque required for this study at the motor shaft. An AC motor speed control system governs the turbine rotational speed to desired set values. A digital wave rotary torque transducer is placed between the motor and the vertical shaft and measures the torque on the turbine shaft at the rate of 200 Hz to the maximum value of 5 N · m. It also has a rotational speed sensor with user adjustable range that enables direct measurement of the turbine power. The torque transducer records a negative value when the turbine generates power and tends to spin the motor faster. A positive torque shows that the turbine operates at the beginning or end of the power curve where, due to stall or high drag of the blades, the turbine generates less power and the motor drives the turbine.

A miniature universal strain gauge load cell capable of measuring forces up to 100 N enables measurement of the thrust force on the turbine rotor. Needles of 0.7 mm diameter used as rollers between base plate of the test rig and the tunnel rim along with lubrication of the contact surfaces minimize the surface friction and allow the rig to smoothly slide on the tunnel rim. An aluminum flat bar clamped to the water tunnel rim secures the load cell attached to the rig base plate. Schematic of the load cell attached to the rig and position of the rollers is depicted in Fig. 4. In addition to torque and thrust measurements, an Acoustic Doppler Velocimeter measures the undisturbed flow velocity at the inlet of the test section at the rate of 200 Hz.

3. Test procedure and data analysis

Tests start for the model turbine without a shroud in selected flow speeds of 0.7, 0.9, and 1.1 m/s. This corresponds to the

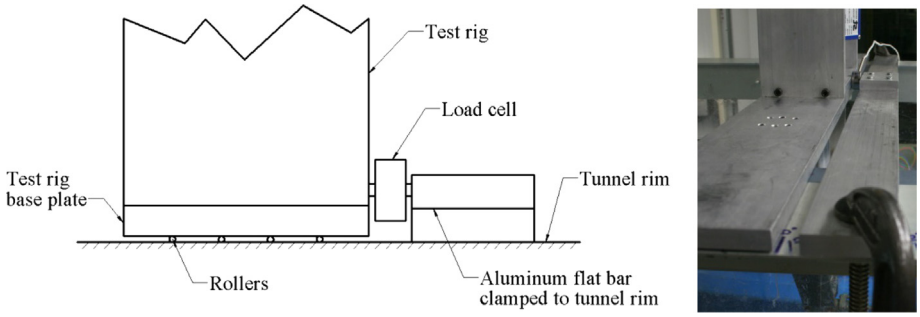

Fig. 4. Schematic of the test rig and the load cell secured between the base plate and clamped flat bar (left). The rollers and thoroughly lubricated surfaces allow for a smooth slide of the rig on the tunnel upper rim (right).

Reynolds numbers of 1.38×10^5, 1.77×10^5, and 2.17×10^5 based on the rotor diameter and flow velocity. Turbulence intensity of the flow ranges from 2.06 to 2.89, as calculated from the ADV measurements. The torque exerted on the turbine rotor is measured at each Reynolds number for the range of tip speed ratio, *TSR*, investigated in the performance curve. This is then repeated for the model turbine with the shroud and then with the diffuser placed around the rotor blade. The drag force on the turbine structure is measured at each test velocity and the thrust force on the turbine is then calculated by subtracting this drag force from the total axial force measured on the turbine. For a given flow speed and rotor angular velocity, the measured torque and thrust is averaged and corrected for zero offset. Then *TSR* and coefficients of power, C_P, and thrust, C_T, are calculated as follows:

$$TSR=\frac{R\omega}{V} \tag{1}$$

$$C_P=\frac{Q\omega}{1/2\rho AV^3} \tag{2}$$

$$C_T=\frac{T}{1/2\rho AV^2} \tag{3}$$

where Q and T are the torque and thrust of the turbine and ω and V are respectively the angular velocity of the turbine shaft and the flow speed. The power and thrust coefficients are calculated based on the swept area of the rotor blade, A. Fig. 5 shows the model turbine with the shroud and the diffuser in the water tunnel during an experiment.

4. Blockage correction

Placing a turbine in a wind or water tunnel partially blocks the flow passage of the tunnel test section. This increases the flow velocity upstream of the turbine which results in increased measured torque and thrust. Therefore, turbine performance obtained in a partially blocked flow needs correction to represent performance of the turbine in an unbounded free stream. In this work the velocity correction used by Bahaj et al. (2007) is employed along with the model proposed by Whelan et al. (2009) which accounts for the free surface proximity and blockage effects. Bahaj et al. employed the method of Barnsley and Wellicome (1990) who modified the Glauert's (1947) equations for wake expansion of a wind turbine. The method is based on an actuator disk model where flow is assumed to be inviscid and uniform across cross sections of the streamtube enclosing the turbine disk. A uniform thrust on the disk is result of the assumed pressure drop across it. The model leads to the equivalent open water or free stream velocity V_F as follows:

$$\frac{V}{V_F}=\frac{\beta}{\beta^2+C_T^T/4} \tag{4}$$

where C_T^T is the thrust coefficient calculated from water tunnel measurements and β is the ratio of the flow speed across the disk to the tunnel velocity, V. Bahaj et al. find β in an iterative manner using two equations derived from conservation of mass and momentum principles applied to a wall bounded flow over the actuator disk. The equations used to find β relate the blockage ratio, B, the ratio of bypass flow to the tunnel velocity, τ, and the ratio of flow speed far downstream of the disk to the tunnel velocity, α. Blockage ratio is the ratio of the disk area to the flow cross section area and the bypass flow is the portion of flow outside the streamtube containing the turbine disk. Bahaj et al. then use the velocity ratio, Eq. (4), to correct the power and thrust coefficients as well as the *TSR* as follows:

$$C_P=C_P^T\left(\frac{V}{V_F}\right)^3 \tag{5}$$

$$C_T=C_T^T\left(\frac{V}{V_F}\right)^2 \tag{6}$$

$$TSR=TSR^T\left(\frac{V}{V_F}\right) \tag{7}$$

where C_P^T and TSR^T are values calculated from water tunnel measurements. In this work we obtain β from the model proposed by Whelan et al. (2009) that accounts for the free surface proximity as well as the wall blockage effect. Whelan et al. extend

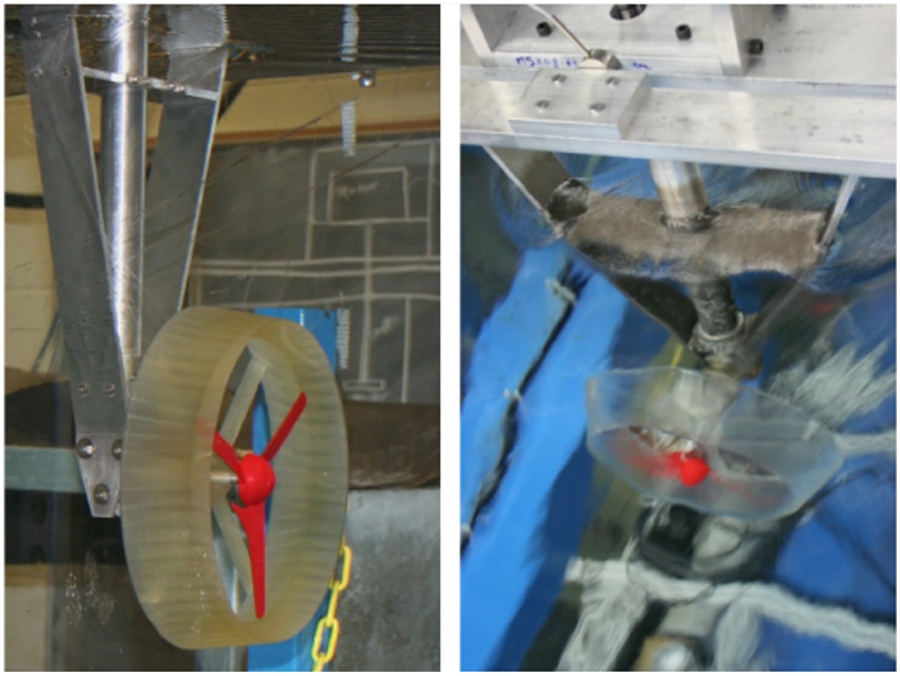

Fig. 5. The model turbine with the shroud (left) and top view of the turbine with the diffuser (right) in the water tunnel during an experiment.

the one-dimensional actuator disk analysis of Garrett and Cummins (2007), which considers turbine flows constrained between two rigid surfaces, to allow for the deformation of the free surface. Deformation of the free surface is due to the pressure change in the region of the turbine and is associated with the flow Froude number. Combining the continuity, Bernoulli, and momentum equations Whelan et al. derive a quartic equation in terms of the bypass flow velocity ratio τ as follows:

$$Fr^2\tau^4+4\alpha Fr^2\tau^3+(4B-4-2Fr^2)\tau^2+(8-8\alpha-4Fr^2\alpha)\tau + (8\alpha-4+Fr^2-4\alpha^2B)=0 \quad (8)$$

in which $Fr=V/\sqrt{gH}$ is the upstream Froude number with g the gravity and H the upstream water level. This equation gives real solutions of τ for certain range of Fr, B, and α for which the bypass flow remains subcritical. Obtaining τ and α from the solution of Eq. (8), the thrust coefficient is then calculated as:

$$C_T=\tau^2-\alpha^2 \quad (9)$$

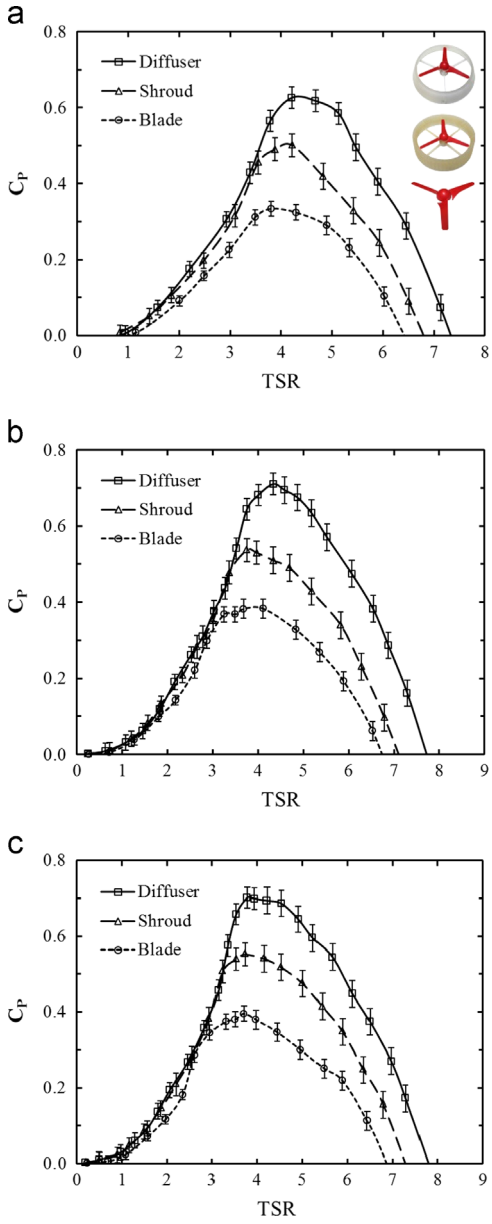

Fig. 6. Performance curves of the model turbine with and without shrouds at flow speeds of (a) 0.7 m/s, (b) 0.9 m/s, and (c) 1.1 m/s.

and the ratio of the flow speed across the disk to the tunnel velocity is given by:

$$\beta=\frac{\alpha}{B(\tau-\alpha)}\left[\tau\left(1-\frac{Fr^2}{2}(\tau^2-1)\right)-1\right]. \quad (10)$$

The model is applicable to any device causing a pressure drop in the flow direction. Therefore, we also apply it to the shrouded model turbines provided that the blockage ratio is calculated based on the maximum cross sectional area of the shroud and the diffuser–their exit area. Eq. (8) is solved for the Froude numbers and blockage ratios associated with our experiments and values of C_T and β are then calculated from Eqs. (9) and (10). Froude numbers associated with the experiment flow velocities 0.7, 0.9, and 1.1 m/s are, respectively, 0.29, 0.37, and 0.45. Having found values of β at any corresponding experimental thrust coefficient, Eq. (4) is used to find the equivalent open water velocity. The power and thrust coefficients as well as the *TSR*, are then corrected using Eqs. (5)–(7). As an example, typical thrust coefficient of 0.86 for turbine with the shroud at flow speed of 0.9 m/s results in 2.8% reduction in *TSR*, 5.5% reduction in thrust coefficient, and 8.1% reduction in power coefficient.

5. Uncertainty of measurements

Accuracy of the torque transducer and the load cell is $\pm 0.25\%$ of the full scale. The ADV measures velocity with accuracy of $\pm 0.5\%$ of the measured velocity ± 1 mm/s. Accuracy in the length measurement is ± 0.02 mm. The expanded uncertainty for power and thrust coefficients are calculated based on Type A and Type B standard uncertainty evaluations in accordance to JCGM (2008). Using typical values of $C_P=0.70$ and $C_T=0.78$ for the model turbine with the diffuser at flow speed of 1.1 m/s, the relative combined standard uncertainty is calculated to be respectively 2.15% and 1.28% with the confidence level of approximately 68%. Therefore for the stated example $C_P=0.70\pm 0.03$ and $C_T=0.78\pm 0.02$ and the reported expanded uncertainty is based on the standard uncertainty multiplied by a coverage factor of 2 providing a level of confidence of approximately 95%. For the purpose of clarity, error bars are only added to selected figures.

6. Results and discussion

Figs. 6 and 7 show the power and thrust coefficients of the model turbine obtained in the water tunnel experiments and plotted against tip speed ratio. Coefficients are calculated based on the blade swept area. Results are for the bare turbine, turbine with the shroud, and turbine with the diffuser. The three configurations respectively referred to as the blade, the shroud, and the diffuser in the diagrams. The experimental data for this study can be downloaded from Shahsavarifard and Bibeau (2014).

6.1. Power and thrust coefficients

Fig. 6 shows consistent performance curves with a start at zero, taking a peak at *TSR* of around 4, and descending at around 7 for the three configurations. This reveals the optimal *TSR* of the turbine to be approximately at the middle of the performance curve. The same and consistent trend of performance enhancement is seen for the unshrouded turbine in the three diagrams when the shroud and the diffuser are added: the shroud increases power of the turbine to some extent while the diffuser shows the most effectiveness. Maximum C_P is 0.33, 0.38, and 0.40 for the bare turbine at flow speeds of 0.7, 0.9, and 1.1 m/s, respectively. Maximum power coefficients increase to 0.50, 0.54, and, 0.55 with

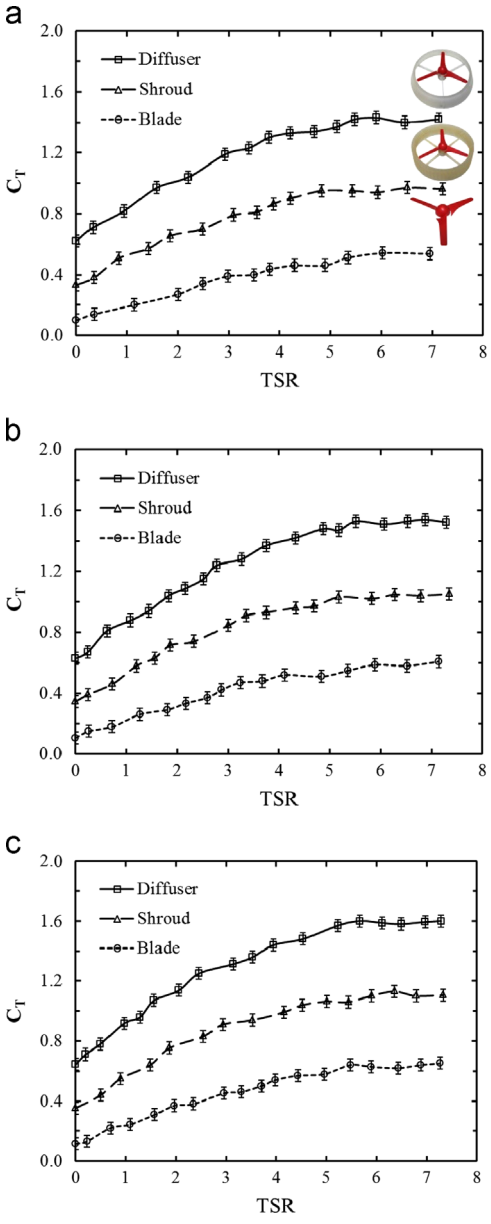

Fig. 7. Thrust coefficient curves of the model turbine with and without shrouds at flow speeds of (a) 0.7 m/s, (b) 0.9 m/s, and (c) 1.1 m/s.

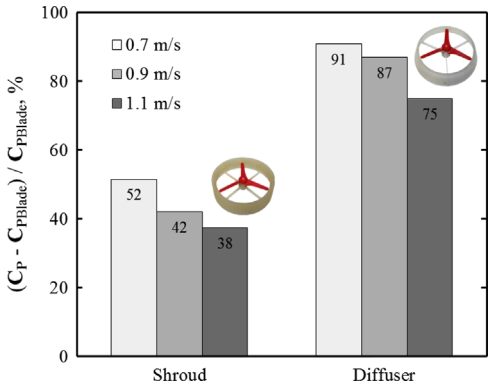

Fig. 8. Relative increase in the maximum power coefficients of the shrouded turbine over the bare turbine.

the shroud, and to 0.63, 0.71, and, 0.70 with the diffuser. It is also observed that placing a shroud on the turbine tends to displace the peak value of the curve to higher tip speed ratios. This behaviour has been also reported by other authors (Phillips et al., 1999). The more power enhancement the larger the shift: maximum C_P of the diffuser occurs at higher *TSR* than that of the shroud and maximum C_P of the shroud is at higher *TSR* than that of the blade. At a constant flow speed, working at higher tip speed ratio translates to higher angular velocity of the turbine shaft. This is an advantage for the operation of turbine generator (Shives and Crawford, 2011). The maximum power coefficient for a hydrokinetic turbine occurs at an optimum tip speed ratio where due to the appropriate angle of attack at the blades the maximum lift is generated. At lower tip speed ratios lift force drops significantly and stall occurs due to high angles of attack at the blades. The low power coefficients at high tip speed ratios however is due to the increased drag caused by low angles of attack (Burton et al., 2001).

One functionality of a shroud placed around the turbine rotor as explained earlier is to increase the flow velocity through the rotor plane. This increase in the flow velocity consequently increases the angle of attack at the blades. At low tip speed ratios this increase in angle of attack intensifies the stall condition and hence no power enhancement occurs. This is seen in the performance curves of Fig. 6 where the low tip speed ratio portion of the curves for the blade, the shroud, and the diffuser fall on each other and shrouds are unable to increase the power. However at high tip speed ratios, increasing the angle of attack decreases the drag on the blade and performance enhancement occurs. This is observed in Fig. 6 where using the shroud and the diffuser increases the high tip speed ratio portion of the performance curve of the turbine.

Fig. 7 is the thrust coefficient curves corresponding to the performance curves shown in Fig. 6. Here also the results are consistent where the thrust force starts from a minimum value when the turbine is stopped and then ascends as the *TSR* increases. The rotor blade at rest has the minimum frontal area in comparison to the turbine with the shroud and with the diffuser and hence creates the least blockade to the flow. This explains the lower drag force for the bare turbine at zero rpm. By increasing the *TSR*, the rotor becomes more impermeable to the flow and the thrust coefficient increases. Thrust coefficient of a rotor can reach values as high as the drag coefficient of a circular disk, 1.17, in sufficiently high tip speed ratios, or as high as 2.0 for heavily loaded rotors (Manwell et al., 2009). Results for thrust and power are consistent: the bare turbine with the least thrust force has the lowest performance and the turbine with the shroud and with the diffuser having higher thrusts achieves higher power coefficients. Unlike the performance curve which has a maximum at an optimum *TSR* and lower power coefficients before and after that point, the thrust force has an ascending behaviour. As power is the thrust force times the local velocity at the rotor plane, the maximum power occurs where this product is the highest. Although thrust continues increasing at high *TSR*, the flow velocity at the rotor decreases due to the increased blockade resulting from a higher rotor speed. Therefore, the maximum power does not occur at the maximum thrust.

Fig. 8 shows the relative increase in the maximum power coefficient of the two shrouded turbines with respect to the unshrouded turbine. The model turbine experiences 52%, 42%, and 38% relative increase in the maximum power coefficient with the shroud, and 91%, 87%, and 75% relative increase with the diffuser at the respective flow speeds of 0.7, 0.9, and 1.1 m/s. Both the shroud and the diffuser have their maximum effect on the power at flow speed of 0.7 m/s. The power enhancement by the shroud and the diffuser decreases at higher flow velocities. Power enhancement by the shroud and the diffuser at 0.7 m/s is

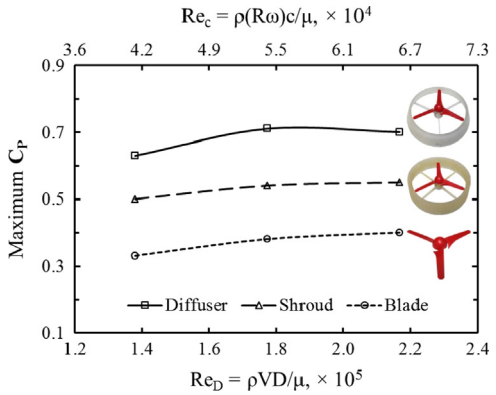

Fig. 9. Maximum power coefficients of the model turbine with and without shrouds against Reynolds number.

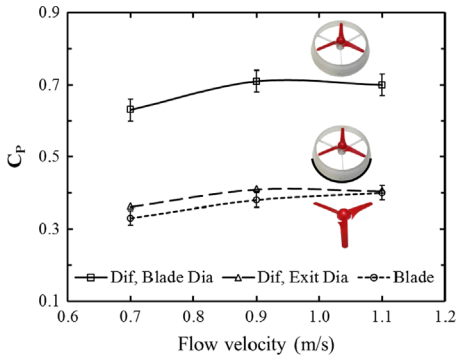

Fig. 10. Maximum power coefficients of the model turbine with and without the diffuser calculated based on the blade swept area and the diffuser exit area.

respectively 14% and 16% more than their enhancement at 1.1 m/s flow velocity. This result indicates the higher effectiveness of shrouded turbines in low speed currents and that the power enhancement of a shroud decreases at faster streams.

6.2. Reynolds number effect

Maximum power coefficients of the model turbine with and without shrouds are plotted against Reynolds number in Fig. 9. The bottom axis is the rotor diameter Reynolds number computed from the flow velocity and rotor diameter. The top axis is the chord Reynolds number calculated with the chord length of the blade at 60% spanwise location and the blade tip speed. Maximum power coefficients show the same increase trend with *Re* for the unshrouded and shrouded turbines. This rate of increase of the maximum C_P, however, decreases with *Re* and it is expected that the maximum C_P does not change at higher Reynolds numbers. This aspect could not be tested. This indicates that the maximum achievable C_P of the model turbine with the diffuser is 0.7 and relatively less gain would occur at higher Reynolds numbers.

For experiments on a model turbine to realistically simulate performance of a full scale turbine two conditions need to be met. Ideally the Reynolds number and tip speed ratio must remain the same for the field and water tunnel experiments. The condition on the tip speed ratio is the one that is met in nearly all of the wind or water tunnel experiments (Adaramola and Krogstad, 2011). Meeting this condition, it is then impossible to preserve the Reynolds number of a full scale turbine test. While the tip speed ratio is conserved, the Reynolds number could be one or two orders of magnitude larger for a full scale turbine (Wilson, 2009). A recommended range of Reynolds number required for a reliable comparison of a model turbine and a full scale turbine is 10^5 (de Vries, 1983). This criterion has been met in all of our experiments therefore it is assumed that the results of this study remain valid for higher Reynolds numbers of full scale experiments.

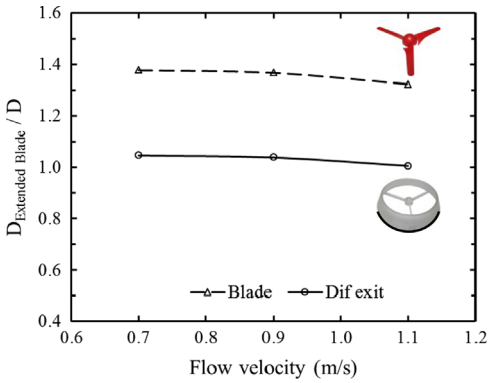

Fig. 11. Diameter of the extended blade for generating the same power as the model hydrokinetic turbine with the diffuser.

6.3. Extended blade

Performance coefficients in the foregoing discussions are calculated based on the swept area of the blade which is the reason for exceeding the Betz limit with the diffuser. This is indeed comparing the output power of the turbine to the kinetic power of the stream available for the rotor swept area. It is beneficial and more realistic from an industrial application to compare the performance of a shrouded turbine to the available kinetic power for the largest area of shroud, the exit area. In this manner comparison is in fact between performances of a shrouded turbine and an unshrouded turbine with a rotor that has a diameter as large as the shroud exit diameter. The discussion in this section focuses on the turbine with the diffuser, as the diffuser demonstrates the most performance enhancement.

Fig. 10 shows the maximum power coefficients of the unshrouded turbine and also the turbine with the diffuser. Performance coefficients for the model turbine with the diffuser are calculated based on the diffuser exit diameter. The top and the middle lines in the diagram represent the maximum power coefficients of the turbine with the diffuser calculated with the rotor swept area and the diffuser exit area, respectively. The bottom line is the maximum power coefficient of the unshrouded turbine. It is only the top line that exceeds the 0.59 Betz limit and power coefficients calculated with the diffuser exit area are below the theoretical limit, as expected. Comparing the middle and bottom lines shows that the maximum power coefficients of the turbine with the diffuser, based on the diffuser exit area, exceeds the unshrouded turbine performance by 9% and 8% at flow speeds of 0.7 and 0.9 m/s, respectively. At a flow of 1.1 m/s it implies that, an unshrouded turbine with the same power characteristics as the blade and of the size equal to the diffuser exit diameter generates within 1% as much power as the model turbine with the diffuser.

Next, the diameter of an extended rotor blade capable of generating the same power as the model turbine with the diffuser is calculated. The assumption is that the extended rotor blade is a geometrically scaled up turbine with the same power coefficient. Using power coefficients of the rotor blade and maximum power of turbine with the diffuser allows calculation of the extended blade diameter. Fig. 11 shows ratio of the extended blade diameter to diameter of the rotor blade as well as the diffuser exit diameter. The top line is diameter ratio of the extended blade and the rotor blade with values of 1.38, 1.37, and 1.32 at the experiment flow velocities 0.7, 0.9, and 1.1 m/s, respectively. Results indicate that an extended blade requires 38%, 37%, and 32% larger diameter than the blade in the respective velocities to generate the same amount of power as the model turbine with the diffuser does. The bottom

line in the figure is the ratio of the extended blade diameter to the diffuser exit diameter with values of 1.05, 1.04, and 1.01. Similarly, an extended blade with 5%, 4%, and 1% larger diameter than the diffuser exit diameter generates the same power as the model turbine with the diffuser in the respective flow speeds. On average, this is a rotor blade with only 3% larger diameter than the diffuser exit diameter. This is in agreement with van Bussel (2007, 1999) who explains this result using his momentum theory (van Bussel, 1998). Assuming no viscous wake mixing behind the diffuser, van Bussel states that the power of a shrouded wind turbine increases as a result of increased mass flow through the rotor blade, and that the amount of energy extracted per unit volume with a shrouded and an unshrouded wind turbine is the same. He concludes that the achievable performance of a diffuser augmented wind turbine is comparable to the performance of an unshrouded turbine having a diameter equal to the diffuser exit diameter. This has been also observed by Scherillo et al. (2011) in their experimental study on a streamlined diffuser with 26° half angle. They conclude that the contribution of a diffuser to the power coefficient of a turbine is relatively small, 7.5%, when the C_P is calculated based on the diffuser exit area.

6.4. Shroud or extended blade

Fig. 12 compares the volume of an extended rotor blade and that of the blade with the diffuser for the model hydrokinetic turbine. This provides an estimation of the size for the two configurations: the model hydrokinetic turbine with the blade and the diffuser and one with an extended blade. It is seen that the extended blade in the three flow velocities has on average 2.5 times larger volume than the basic rotor blade. In contrast, the rotor blade and diffuser volume is 28 times greater than that of the basic rotor blade alone. This means that the model turbine with the diffuser has 11 times larger volume than the model turbine with the extended blade.

This result is important when it comes to the industrial manufacturing of hydrokinetic turbines as less material normally leads to lower product cost. Since an extended blade can substitute for a blade and a diffuser, employing a shrouded turbine may not be justified for just increasing performance of the turbine: it needs to benefit the hydrokinetic turbine system in other ways. This statement is in contrast to many literature studies that highlight the apparent increase in the power coefficient as the main motivation factor.

Benefits of a shroud include reducing the destructive effect on the performance when the rotor blades pass too close to the flow boundaries (Fraenkel, 2002). This happens in shallow water streams or when turbines need to be deployed close to the water surface or on the riverbed. A shroud enclosing the rotor prevents the counter-productive effect of the surface on the turbine performance. A shroud

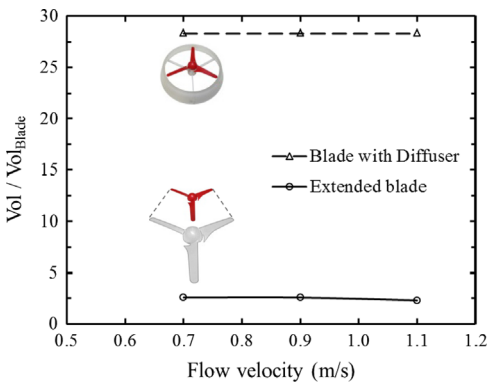

Fig. 12. Comparison of volumes for the model turbine with the diffuser and with the extended blade generating the same power.

can secure the turbine generator and powertrain and also can be used as the structure to install the turbine on the riverbed, or as the buoy to float it in the stream (Khan et al., 2009). Significant advantage in the powertrain design can be obtained with a shroud when striving, for example, to avoid the use of a gearbox to reduce maintenance and eliminate oil spillage to facilitate the hydrokinetic permitting process. Additionally, a shroud can benefit the marine life, providing protection for fish or diving birds from entering the rotor from the sides. A turbine with a smaller rotor blade encased in a shroud may have less impact on marine species compared to a larger unprotected rotating blade. In off-axis flow conditions, a shroud results in less performance deterioration by streamlining the flow through the rotor blade. This aspect will be studied in detail in a future article by the present authors. Shrouds, however, can make hydrokinetic turbine deployment and retrieval more difficult, impact on water safety for operators, and produce a larger wake region impacting aquatic life, especially when the flow is not aligned with the turbine axis–possibly affecting how turbine farms placement are approved for permitting.

Selecting either of the approaches, a smaller blade with a shroud or a larger blade, requires optimization on multiple variables, not well documented, with the fabrication, deployment and retrieval, maintenance, overall cost, water depth, flow velocity, and marine life part of the optimization. Although utilizing a larger rotor blade without a shroud might seem a lower cost approach, a smaller blade with a shroud could be a better option for sites with low velocities, shallow water, a maintenance free powertrain design, and where marine life safety is of concern.

7. Conclusions

A 19.8 cm diameter horizontal axis hydrokinetic model turbine and two shrouds are designed, manufactured and experimentally tested in the water tunnel facility at the University of Manitoba. Consistent power and thrust curves for the model turbine with and without the shrouds are obtained over the performance curve range. Free surface proximity and blockage effects are corrected using a one dimensional actuator disk model. A maximum power enhancement of 91% over the unshrouded turbine is obtained with the straight wall diffuser design. Maximum power coefficients are seen to increase with the Reynolds number but at a decreasing rate. It is observed that a shroud is more effective in low speed water currents. Power coefficients calculated based on the exit area of the diffuser is found comparable to that of the unshrouded turbine with the size of the diffuser exit diameter. This is in agreement with van Bussel momentum theory, which states that the achievable power for a diffuser augmented wind turbine is comparable with the power of a bare turbine with the size of diffuser exit diameter. It is also found that at flow speeds exceeding 1 m/s, an extended blade having a diameter equal to the exit diameter of the diffuser generates the same power as the model turbine with the diffuser. An extended blade can substitute for a smaller blade with diffuser and generates the same power, which could be considered as a superior choice for the industry. However, a smaller shrouded blade can be a better choice for low speed flow sites, shallow water currents, and where marine life is of concern. Unlike wind applications, the case to use a shroud for hydrokinetic power generation could be justifiable based on the system optimization, and not by the apparent increase in the power coefficient.

Acknowledgment

Support for this research is provided by the NSERC/Manitoba Hydro Chair in Alterative Energy. We would like to acknowledge the support of Tom Molinski and Jeff Blais from Manitoba Hydro.

References

Adaramola, M.S., Krogstad, P-Å., 2011. Experimental investigation of wake effects on wind turbine performance. Renewable Energy 36, 2078–2086.

Alfredsson, P-H., Dahlberg, J-Å, 1979. A Preliminary Wind Tunnel Study of Windmill Wake Dispersion in Various Flow Conditions. Technical Note AU-1499, Part 7, FFA. Stockholm, Sweden.

Bahaj, A.S., Molland, A.F., Chaplin, J.R., Batten, W.M.J., 2007. Power and thrust measurements of marine current turbines under various hydrodynamic flow conditions in a cavitation tunnel and a towing tank. Renewable Energy 32, 407–426.

Barnsley, M.J., Wellicome, J.F., 1990. Final Report on the 2nd Phase of Development and Testing of a Horizontal Axis Wind Turbine Test Rig for the Investigation of Stall Regulation Aerodynamics. Carried out under ETSU Agreement E.5A/CON5103/1746.

Birjandi, A.H., Bibeau, E.L., Chatoorgoon, V., Kumar, A., 2013. Power measurement of hydrokinetic turbines with free-surface and blockage effect. Ocean Eng. 69, 9–17.

Burton, T., Sharpe, D., Jenkins, N., Bossanyi, E., 2001. Wind Energy Handbook. Wiley, New York, NY.

de Vries, O., 1983. On the theory of the horizontal-axis wind turbine. Annu. Rev. Fluid Mech. 15, 77–96.

Drouen, L., Charpentier, J.F., Semail, E., Clenet, S., 2007. Study of an innovative electrical machine fitted to marine current turbines. In: OCEANS 2007 Europe Conference, pp. 1–6.

Ebert, P.R., Wood, D.H., 1997. The near wake of a model horizontal-axis wind turbine—I. Experimental arrangements and initial results. Renewable Energy 12, 225–243.

Ebert, P.R., Wood, D.H., 2002. The near wake of a model horizontal-axis wind turbine at runaway. Renewable Energy 25, 41–54.

Fraenkel, P.L., 2002. Power from marine currents. Proc. Inst. Mech. Eng. Part A J. Power Energy 216, 1–14.

Gaden, D.L.F., 2007. An Investigation of River Kinetic Turbines: Performance Enhancements, Turbine Modelling Techniques, and an Assessment of Turbulence Models. University of Manitoba.

Gaden, D.L.F., Bibeau, E.L., 2010. A numerical investigation into the effect of diffusers on the performance of hydro kinetic turbines using a validated momentum source turbine model. Renewable Energy 35, 1152–1158.

Garrett, C., Cummins, P., 2007. The efficiency of a turbine in a tidal channel. J. Fluid Mech. 588, 243–251.

Glauert, H., 1947. The Elements of Aerofoil and Airscrew Theory, second ed. Cambridge University Press, New York, NY.

Haans, W., Sant, T., van Kuik, G., van Bussel, G., 2005. Measurement of tip vortex paths in the wake of a HAWT under yawed flow conditions. J. Sol. Energy Eng. 127, 456–463.

Hansen, M.O.L., Sørensen, N.N., Flay, R.G.J., 2000. Effect of placing a diffuser around a wind turbine. Wind Energy 3, 207–213.

Isensee, G.M., Abdul-Razzak, H., 2012. Modeling and analysis of diffuser augmented wind turbine. Int. J. Energy Sci 2, 84–88.

JCGM, 2008. Evaluation of Measurement Data—Guide to the Expression of Uncertainty in Measurement, JCGM 100:2008 (GUM 1995 with minor corrections). ⟨http://www.bipm.org/utils/common/documents/jcgm/JCGM_100_2008_E.pdf⟩.

Khan, M.J., Bhuyan, G., Iqbal, M.T., Quaicoe, J.E., 2009. Hydrokinetic energy conversion systems and assessment of horizontal and vertical axis turbines for river and tidal applications: A technology status review. Appl. Energy 86, 1823–1835.

Khan, M.J., Iqbal, M.T., Quaicoe, J.E., 2008. River current energy conversion systems: Progress, prospects and challenges. Renewable Sustainable Energy Rev. 12, 2177–2193.

Lawn, C.J., 2003. Optimization of the power output from ducted turbines. Proc. Inst. Mech. Eng. Part A J. Power Energy 217, 107–117.

Lilley, G.M., Rainbird, W.J., 1956. A Preliminary Report on the Design and Performance of a Ducted Windmill. College of Aeronautics, Cranfield, UK (Report 102).

Lokocz, T.A., 2012. Testing of a Ducted Axial Flow Tidal Turbine. University of Maine.

Manwell, J.F., McGowan, J.G., Rogers, A.L., 2009. Wind Energy Explained: Theory Design and Application. second ed. Wiley, UK.

Massouh, F., Dobrev, I., 2007. Exploration of the vortex wake behind of wind turbine rotor. J. Phys. Conf. Ser 75, 012036.

Myers, L., Bahaj, A.S., 2006. Power output performance characteristics of a horizontal axis marine current turbine. Renewable Energy 31, 197–208.

O Rourke, F., Boyle, F., Reynolds, A., 2010. Tidal energy update 2009. Appl. Energy 87, 398–409.

Ohya, Y., Karasudani, T., Sakurai, A., Abe, K., Inoue, M., 2008. Development of a shrouded wind turbine with a flanged diffuser. J. Wind Eng. Ind. Aerodyn. 96, 524–539.

Phillips, D.G., 2003. An Investigation on Diffuser Augmented Wind Turbine Design. The University of Auckland.

Phillips, D.G., Nash, T.A., Oakey, A., Flay, R.G.J., Richards, P.J., 1999. Computational fluid dynamic and wind tunnel modelling of a diffuser augmented wind turbine. Wind Eng 23 (1), 7–13.

Scherillo, F., Maisto, U., Troise, G., Coiro, D.P., Miranda, S., 2011. Numerical and experimental analysis of a shrouded hydroturbine. In: International Conference on Clean Electrical Power (ICCEP), pp. 216–222.

Shahsavarifard, M., Bibeau, E.L., 2014. Experimental Power and Thrust Coefficients of a Shrouded Horizontal Axis Hydrokinetic Turbine. doi:10.5203/ds_sha_1.

Shives, M., Crawford, C., 2011. Developing an empirical model for ducted tidal turbine performance using numerical simulation results. Proc. Inst. Mech. Eng. Part A J. Power Energy 226 (1), 112–125.

ten Hoopen, P.D.C., 2009. An Experimental and Computational Investigation of a Diffuser Augmented Wind Turbine with an Application of Vortex Generators on the Diffuser Trailing Edge. Delft University of Technology.

van Bussel, G.J.W., 1998. Development of a Momentum Theory for DAWT's (Diffuser Augmented Wind Turbines). Mie University, Tsu, Japan.

van Bussel, G.J.W., 1999. An assessment of the performance of diffuser augmented wind turbines (DAWT's). In: 3rd ASME/JSME Joint Fluids Engineering Conference, San Francisco, USA.

van Bussel, G.J.W., 2007. The science of making more torque from wind: Diffuser experiments and theory revisited. J. Phys. Conf. Ser 75, 012010.

van Holten, Th., 1981. Concentrator systems for wind energy, with emphasis on tipvanes. Wind Eng 5 (1), 29–45.

Vermeer, L.J., 2001. A review of wind turbine wake research at TUDelft. In: A Collection of the 2001 ASME Wind Energy Symposium Technical Papers. ASME, New York, pp. 103–113.

Vermeer, L.J., Sørensen, J.N., Crespo, A., 2003. Wind turbine wake aerodynamics. Prog. Aerosp. Sci. 39, 467–510.

Whelan, J.I., Graham, J.M.R., Peiró, J., 2009. A free-surface and blockage correction for tidal turbines. J. Fluid Mech. 624, 281–291.

Wilson, R.E., 2009. Wind Turbine Technology: Fundamental Concepts of Wind Turbine Engineering, second ed. ASME Press.